JVI Journals.ASM.org

Impact on the Endoplasmic Reticulum and Golgi Apparatus of Turnip Mosaic Virus Infection

Romain Grangeon,[a] Maxime Agbeci,[a] Jun Chen,[b] Gilles Grondin,[c] Huanquan Zheng,[b] and Jean-François Laliberté[a]

INRS-Institut Armand-Frappier, Institut National de la Recherche Scientifique, Laval, Québec, Canada[a]; Department of Biology, McGill University, Montréal, Québec, Canada[b]; and Département de Biologie, Université de Sherbrooke, Sherbrooke, Québec, Canada[c]

The impact of turnip mosaic virus (TuMV) infection on the endomembranes of the host early secretory pathway was investigated using an infectious clone that has been engineered for tagging viral membrane structures with a fluorescent protein fused to the viral protein $6K_2$. TuMV infection led to the amalgamation of the endoplasmic reticulum (ER), Golgi apparatus, COPII coatamers, and chloroplasts into a perinuclear globular structure that also contained viral proteins. One consequence of TuMV infection was that protein secretion was blocked at the ER-Golgi interface. Fluorescence recovery after photobleaching (FRAP) experiments indicated that the perinuclear structure cannot be restocked in viral components but was dynamically connected to the bulk of the Golgi apparatus and the ER. Experiments with $6K_2$ fused to photoactivable green fluorescent protein (GFP) showed that production of motile peripheral $6K_2$ vesicles was functionally linked to the perinuclear structure. Disruption of the early secretory pathway did not prevent the formation of the perinuclear globular structure, enhanced the clustering of peripheral $6K_2$ vesicles with COPII coatamers, and led to inhibition of cell-to-cell virus movement. This suggests that a functional secretory pathway is not required for the formation of the TuMV perinuclear globular structure and peripheral vesicles but is needed for successful viral intercellular propagation.

Vertebrate positive-strand RNA viruses are known to remodel the endomembrane system of the host cell (for a review, see references 16 and 42). These membrane alterations are associated with the viral RNA replication complex, and the resulting organization has been given the name virus factory. Electron tomography has been used to generate three-dimensional images of virus-induced alterations (for a review, see reference 19). Analyses of coronavirus, dengue virus, and picornavirus factories (8, 27, 34, 58) have revealed a reticulovesicular/tubular network of modified endoplasmic reticulum (ER) that integrates convoluted membranes, numerous double-membrane vesicles (DMVs) that may be interconnected, and vesicle packets that apparently arise from the merging of DMVs. The biogenesis of these virus factories affects the function of the host secretory pathway by interacting with or interfering with cellular membrane trafficking proteins in the case of the Norwalk virus (50), foot-and-mouth disease virus (37), and poliovirus (6, 7). In the past, research on vertebrate virus infection suggests that the modifications of the host secretory pathway usually result from the action of one or two viral proteins (52, 60). Generally, these viral proteins have one or several transmembrane domains that consist of stretches of approximately 20 hydrophobic amino acid residues. They also possess other molecular determinants that interact with host components necessary for the subversion of the host secretory pathway (6, 7, 24, 37, 50).

Membrane rearrangements involving the ER have also been observed in virus-infected plant cells (for a review, see references 29 and 55). These virus-induced cellular alterations are required for viral genome replication or for virus cell-to-cell movement. The modifications generally involve the formation of spherules, vesicles, and/or multivesicular bodies, which may be bound by a double-layer membrane and are often connected by a narrow channel to the surrounding cytosol. However, there are fundamental differences in the endomembrane system between plant and animal cells. In animal cells, the ER is tightly associated with microtubules, and Golgi bodies are clustered at the microtubule-organizing centers (MTOCs) near the nucleus. In plant cells, the ER is associated with actin microfilaments, and no MTOCs have been found near the nuclei. Furthermore, Golgi stacks in plant cells are not clustered but are singly distributed throughout the cytoplasm and are in close association with highly dynamic interconnected ER tubules and actin tracks (9, 36, 39, 51). Plant cells are also characterized by the presence of plasmodesmata that provide cytoplasmic continuity between adjacent cells. These plasma membrane-lined channels contain ER-derived desmotubules and actin filaments and are used for virus cell-to-cell spread (for a review, see reference 44). These distinctive features have been thought to be an underlying reason that may explain the relationship between ER-associated virus replication centers and virus egress, which is exemplified by the observation that tobacco mosaic virus replication takes place in ER-derived compartments that move from cell to cell (26).

It has been shown that infection by tobacco etch virus (TEV) (genus *Potyvirus*) is associated with a vesiculation of the ER network into a series of discrete aggregated structures (48). The viral protein $6K_2$ of TEV is an integral membrane protein and is associated with the punctate structures reminiscent of the structures observed during viral infection (48). Wei and Wang (57) observed in *Nicotiana benthamiana* cells expressing only TEV $6K_2$ fused to the cyan fluorescent protein (CFP) the production of small punctae along with larger ring-like structures. The punctae localized at

Received 11 May 2012 **Accepted** 8 June 2012
Published ahead of print 20 June 2012
Address correspondence to Jean-François Laliberté, jean-francois.laliberte@iaf.inrs.ca.
Supplemental material for this article may be found at http://jvi.asm.org/.

doi:10.1128/JVI.01146-12

endoplasmic reticulum exit sites (ERES), and their formation depended on retrograde and anterograde transport in the ER-Golgi interface (33, 57). Expression of nonfunctional Sar1 and Arf1 mutants, which block the secretory pathway, affected virus yield (57), but the enzyme-linked immunosorbent assay (ELISA) used to measure virus production could not distinguish whether viral RNA synthesis or virus cell-to-cell movement was affected.

Ectopic expression of a single viral protein does not take into consideration the contribution of other viral proteins that are likely to affect the viral process under study. In order to investigate the action of $6K_2$ during infection, an infectious clone of turnip mosaic virus (TuMV) (genus *Potyvirus*) has been engineered to coproduce $6K_2$ as a fluorescent protein (15). The coding sequence of the fluorescent protein was fused with the gene encoding $6K_2$ and inserted between the P1- and HCPro-coding genes as an in-frame translational fusion containing flanking P1 and VPg-Pro cleavage site-coding sequences: $6K_2$-GFP ($6K_2$ fused to green fluorescent protein [GFP])/$6K_2$-mCherry is thus released when the polyprotein is processed during infection. Cytoplasmic fluorescent discrete protein structures were observed in infected *N. benthamiana* cells and contained double-stranded RNA (dsRNA) (a marker for viral RNA replication), the viral proteins VPg-Pro, RNA-dependent RNA polymerase, cytoplasmic inclusion protein (helicase), and host translation factors (15, 17, 25, 53, 56). Similar to what had been noted with the ectopic expression of TEV $6K_2$, the TuMV-induced $6K_2$-tagged vesicles moved along microfilaments and the cortical ER (15) and were additionally associated with chloroplasts (56). Finally, larger irregularly shaped $6K_2$-tagged static structures were found in the midsection of the cell near the nucleus (15, 53). These last structures were not observed after ectopic expression of $6K_2$ only (33, 57).

The above studies focused mainly on the membrane origin and involvement of the secretory pathway and microfilaments on the formation of the $6K_2$-associated vesicular structures. In the present investigation, we looked at the impact TuMV infection has on the overall architecture and dynamics of the early secretory endomembranes. We found that TuMV infection was accompanied by modifications of the ER, COPII coatamers, and Golgi apparatus. We noted that there was an amalgamation of the ER and Golgi apparatus within a perinuclear globular structure, in addition to the generation of motile peripheral viral vesicles associated with the transvacuolar and cortical ER. Experiments with $6K_2$ fused to photoactivable GFP (PAGFP) indicated that the peripheral vesicles were functionally linked to the perinuclear structure. The formation of the perinuclear structure was not dependent on an operational secretory pathway, while the functionality of the peripheral $6K_2$ vesicles and intercellular virus movement were.

MATERIALS AND METHODS

Fluorescent proteins and molecular clones. TuMV infectious clones pCambiaTunos/6KGFP and pCambiaTunos/6KmCherry were described previously (15, 53). The introduction of the 35S-GFP-HDEL gene cassette into pCambiaTunos/6KmCherry was done as follows. pBIN/20-ER-gk (41) was digested with AseI and ligated with similarly digested pCambiaTunos/6KmCherry. Kanamycin-resistant *Escherichia coli* colonies were screened for CambiaTunos/6KmCherry/HDELGFP. To make yellow fluorescent protein (YFP)-Sec24, the gene coding for Sec24A (At3g07100) was amplified from *Arabidopsis thaliana* Col-0 ecotype cDNA library with the following two primers: Sec24-Forward (GGGGACAACTTTGTACAAAAAAGTTGGAATGGGTACGGAGAATCAGGGC) and Sec24-Reverse (GGCGGCCGCACAACTTTGTACAAGAAAGTTGGGTATTAGTTTGTTGAACTTGGCGG). Amplified *Sec24* was cloned into the pDONR222 vector by BP recombination (Gateway cloning). The cloned gene was sequenced and then subcloned into the Gateway compatible destination vector pEarlyGate104 (ABRC stock DB3-686) by LR recombination to yield YFP-Sec24.

$6K_2$ was fused to photoactivable GFP (PAGFP) as follows. Plasmid pMDC32 calnexin fused to PAGFP (CX-PAGFP) (46) was PCR amplified using the forward primer GCTGGATCCGGTGTGAGCAAGGGCGAGGAGCTGTTC (the BamHI site is underlined) and the reverse primer AACTGCAGTTACTTGTACAGCT (the PstI site is underlined). The amplified fragment was digested with BamHI and PstI and ligated with similarly restricted pCambia/$6K_2$ to obtain pCambia/$6K_2$-PAGFP.

Protein expression in plants. Transient expression was performed by agroinfiltration on 3-week-old *N. benthamiana* plants as described in reference 15. The *Agrobacterium tumefaciens* suspension was diluted to an optical density at 600 nm (OD_{600}) of 0.03 for secreted GFP (secGFP) and GFP-HDEL (61), to 0.1 for p24δ1d-YFP (12), ERD2-GFP (47), GFP fused to the transmembrane domain of the rat sialyl transferase (ST-GFP) (9), and YFP-Sec24, to 0.05 for Arf1 constructs (43), and to 0.2 for the viral infectious clones. For coexpression, we agroinfiltrated a 1:1 mixture of the two AGL1 bacteria containing the plasmid of interest. Plants were kept for 3 or 4 days postagroinfiltration (dpa) in a growth chamber until observation.

Brefeldin A (BFA) (Sigma-Aldrich) was used at a final concentration of 10 μg/ml in dimethyl sulfoxide (DMSO). *N. benthamiana* leaves were agroinfiltrated with pCambiaTunos/6KmCherry/HDELGFP or with pCambiaTunos/6KmCherry along with pYFP-Sec24. The leaves were infiltrated with BFA 66 h later and observed by confocal microscopy after a 24-h incubation period.

Confocal microscopy. Agroinfiltrated leaf sections were mounted on a depression microscope slide, aligning the leaf tissue in the well. The cells were observed using a 10× objective, 40×, and/or 63× oil immersion objective on a Radiance 2000 confocal microscope (Bio-Rad) and/or on a LSM 510 Meta confocal microscope (Zeiss). For the Radiance 2000 microscope experiments, an argon-krypton laser was used to excite fluorescent proteins, and for LSM 510 Meta microscope experiments, argon and HeNe lasers were used. Data from both green and red channels were collected at the same time. Photobleaching and photoactivation of GFP was done with a Zeiss LSM 510 Meta system. Ten to fifteen pulses of the 405-nm laser were sufficient to activate PAGFP so that it produced very bright fluorescence emission that was detected by excitation at 488 nm using a 500- to 530-nm band pass filter. A 25-mW blue diode 405-nm laser was used at high output (50 to 100% transmission) to target globular structure or small region in the cytoplasm using the photobleaching function of the Zeiss software in time-lapse mode. Generally, 20 to 30 iterations were enough to bleach fluorescents proteins with the 488-nm laser.

After acquisition, images were processed using Metamorph to quantify the average intensity of fluorescence (6.2r6), and ImageJ (1.46k), Carl Zeiss LSM Image Browser, and/or Adobe Photoshop software for post-capture imaging processes.

Electron microscopy. Transmission electron microscopy (TEM) was performed essentially as described previously (23). Three-week-old *N. benthamiana* leaves were cut into fine pieces (3 mm by 3 mm) using a clean sharp razor blade. Leaves were fixed for 24 h in 2.0% glutaraldehyde, 4% paraformaldehyde, and 0.05% tannic acid in 0.1 M sodium cacodylate buffer (pH 7.4), washed three times in cacodylate buffer, and postfixed in 1% osmium tetroxide in the same buffer for 7 h, washed three times in buffer, and postfixed a second time in 1% osmium tetroxide and 1% potassium ferrocyanide overnight at 4°C. For a control, we rapidly fixed our samples just once in 3% $KMnO_4$ for 4 h, and we observed the same structures but with fewer details, indicating that our fixation method did not induce any artifacts. The samples were washed four times in water, dehydrated in a series of ethanol solutions (30%, 40%, and 50%), and block stained overnight in 1% uranyl acetate in 50% ethanol at 4°C. The samples were dehydrated in ethanol, embedded in Epon 812 resin, and

sliced into thin sections (70 nm thick) with an ultramicrotome Ultracut E of Reichert Jung. In addition, semithin sections (1 μm thick) were stained in toluidine blue for light microscope examination with a Zeiss microscope. Staining of thin sections was performed in 2% aqueous uranyl acetate for 7 min followed by treatment with lead citrate for 3 min. The sections were observed with a TEM Philips 201.

RESULTS

ER, Golgi bodies, COPII coatamers, and chloroplasts are amalgamated in a perinuclear globular structure during TuMV infection. To obtain an overall view of the structural changes that the endomembranes of the early secretory pathway undergo during infection, we examined the distribution of well characterized ER and Golgi organelle markers in TuMV-infected *N. benthamiana* cells by confocal microscopy. We first analyzed the morphology of the ER using GFP-HDEL, a lumenal ER marker (61). In noninfected cells, the marker showed the characteristic cortical polygonal network of short interconnected tubules, transvacuolar strands, and labeling around the nucleus (Fig. 1A). In TuMV-infected cells, the cortical ER did not show any apparent modification, but the ER marker was additionally recruited into a large irregularly shaped globular-like structure juxtaposed to the nucleus in the midsection of the cell that also contained $6K_2$-mCherry (Fig. 1B). The ER was compacted within this structure and did not show a polygonal tubular pattern. Occasionally, the globular structure was distant from the nucleus, or two structures were seen in the same cell. The largest section of this structure was estimated to be 16 μm ± 4 μm long ($n = 30$). By comparison, we calculated the nuclear diameter to be 12 μm ± 3 μm ($n = 30$). The globular structure was linked to the cortical ER by transvacuolar strands (Fig. 1B, white arrowhead), and $6K_2$-mCherry-tagged vesicles essentially devoid of the GFP-HDEL marker were seen traveling along these strands and the polygonal ER tubules (see Movie S1 in the supplemental material). A similar result was obtained with P24σ1d-YFP, a resident membrane ER marker (12) (data not shown).

The morphology of the Golgi apparatus was analyzed using the *cis*-Golgi marker ERD2-GFP (47) and GFP fused to the transmembrane domain of the rat sialyl transferase (ST-GFP) (9), which is targeted to the *trans*-Golgi. In healthy cells, ST-GFP and ERD2-GFP were mainly found as Golgi bodies (9, 47). In TuMV-infected cells, in addition to Golgi bodies, ST-GFP was also localized to a large globular structure near the nucleus (Fig. 1D) that overlapped with the $6K_2$-mCherry fluorescent signal (Fig. 1C). Some individual bodies were seen, but the ST-GFP marker was predominantly diffuse within this structure. The ring-like configuration for some of the $6K_2$-mCherry fluorescent signals denoted the presence of chloroplasts (see below). Similarly, ERD2-GFP was found as individual Golgi bodies (not shown) but was recruited in the globular structure in a diffused form (Fig. 1G) along with $6K_2$-mCherry (Fig. 1F).

Production of punctate motile structures induced by TEV $6K_2$ occurred in a COPII- and COPI-dependent manner (57). We consequently investigated the distribution of the COPII coatamer component Sec24 (18) in the globular structure. YFP-Sec24 in healthy epidermal leaves were characteristically distributed as punctate structures (18). Although the punctate appearance of YFP-Sec24 was still observed in TuMV-infected cells (not observable in Fig. 1H), YFP-Sec24 was also detected in the globular structure induced by the virus (Fig. 1H).

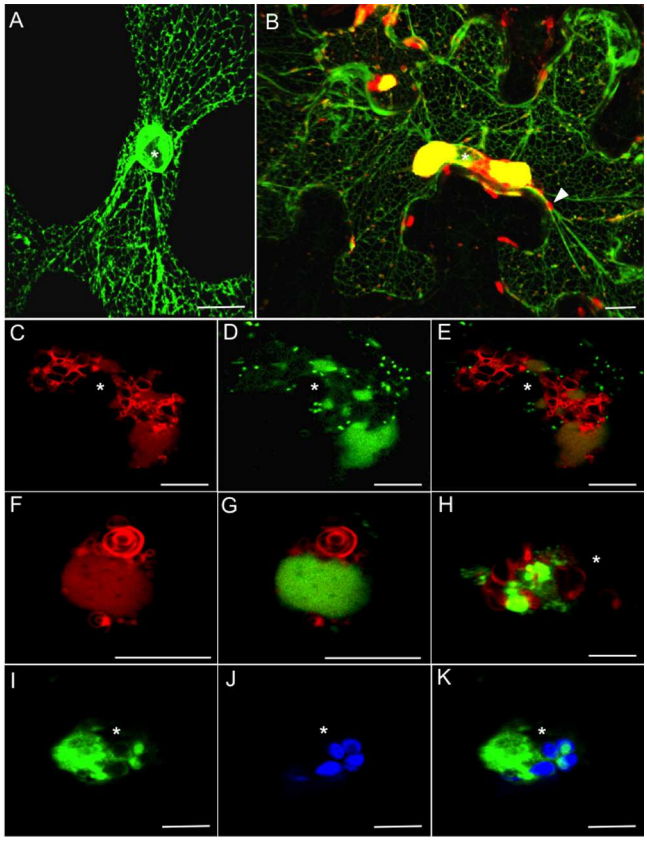

FIG 1 TuMV infection causes amalgamation of endomembranes in the perinuclear area. (A and B) Three-dimensional confocal microscopy images of leaf epidermal cells of *N. benthamiana* showing GFP-HDEL in healthy cells (A) or in TuMV-infected cells expressing $6K_2$-mCherry (B) 4 days after agroinfiltration. The images are three-dimensional renderings of >40 1-μm-thick slices that overlap by 0.5 μm. (C to K) Single optical confocal images showing individual cells infected with TuMV. Panels C to E show coexpressed $6K_2$-mCherry, ST-GFP, and their merged fluorescent signals, respectively. Panels F and G show coexpressed $6K_2$-mCherry and its signal merged with ERD2-GFP signal, respectively. Panel H shows coexpressed $6K_2$-mCherry and its signal merged with YFP-Sec24 signal. Panels I to K show coexpressed $6K_2$-mCherry, chloroplast autofluorescence, and their merged fluorescent signals, respectively. Bars = 10 μm. A white asterisk shows the position of the nucleus, and the white arrowhead points to the transvacuolar ER strand linking the globular structure with cortical ER.

Finally, the presence of chloroplasts in the globular structure was investigated as $6K_2$ vesicles were reported to associate with chloroplasts early in infection (56). Figure 1I to K show that the globular structure contained several chloroplasts, with $6K_2$-GFP labeling their contours.

To analyze the host membrane modifications at the ultrastructural submicron-resolution level, we performed electron microscopy analyses on 4-week-old *N. benthamiana* plants that had been agroinfected with TuMV 6 days before. The structural modifications that were observed cannot be attributed to *Agrobacterium*, since no detectable effect on the morphology of cellular organelles and on the endomembrane network was observed following agroinfiltration with an empty vector (and confirmed in reference 3). Figure 2A shows that infected cells contained characteristic "pinwheel" cytoplasmic inclusion bodies (black arrows) (30) and electron-translucent (+) and electron-opaque (*) vesicles of 90 to

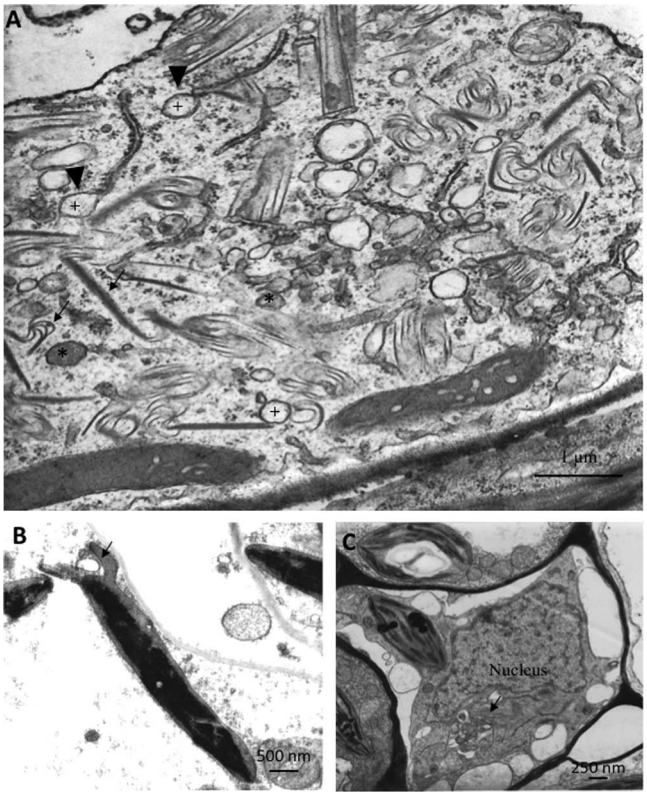

FIG 2 Observations of infected cells by TEM. (A) Cytoplasm of a TuMV-infected cell showing typical inclusion bodies (thin black arrows) and electron-translucent (+) and -opaque (*) vesicles. The large black arrowheads denote vesicles closely associated with tubular ER. (B) Micrograph showing a distorted chloroplast encircling a vesicle (black arrow). (C) Cytoplasm of a TuMV-infected cell with the nucleus close to a cluster of vesicles (black arrow).

340 nm in diameter (average of 170 nm ± 13 nm for 25 vesicles). On some occasions, vesicles were found in direct continuity with tubular ER coated with ribosomes (Fig. 2A, black arrowheads). Some chloroplasts were distorted and formed pseudopodium-like extrusions (Fig. 2B, black arrow), an observation that was previously reported (56). Vesicle clustering in the proximity of the nucleus was also observed (Fig. 2C).

The presence of both lumenal and membrane-associated endomembrane markers in the same $6K_2$-containing globular compartment suggests that the ER, COPII coatamers, and Golgi apparatus are heavily reorganized near the nucleus during TuMV infection, being amalgamated possibly as dense membrane stacks surrounding chloroplasts. On the other hand, the transvacuolar and cortical ER and the rest of the Golgi bodies were not affected.

TuMV infection inhibits protein secretion at the ER-Golgi interface. Because of the amalgamation of the ER and Golgi apparatus into a $6K_2$-tagged globular structure, we investigated the impact of infection on the overall functionality of the host secretory pathway. After its synthesis in the ER, secreted GFP (secGFP) is transported via the Golgi apparatus to the apoplast where its fluorescence is dim. When secretion is inhibited, the protein accumulates intracellularly where it can be readily visualized by fluorescence microscopy (61, 62). Four days following agroinfiltration, we examined *N. benthamiana* leaves for secGFP fluorescence emission by confocal microscopy at a 10× objective magnification (Fig. 3). For a positive control for intracellular retention, we expressed GFP-HDEL. The fluorescence emitted by GFP-HDEL was strong (Fig. 3A), in contrast to the fluorescence of secGFP, which was generally weak or undetectable (Fig. 3B) due to the apoplast acidic pH (61, 62). On the other hand, expression of secGFP in TuMV-infected cells resulted in increased GFP fluorescence (Fig. 3C). We quantified the GFP fluorescence for each treatment using the MetaMorph software, and the data are shown in Fig. 3F. Compared to secGFP alone, we observed higher average intensity fluorescence when secGFP was expressed in infected cells. These data are in agreement with those observed during TEV infection (57). High-magnification observations of secGFP in infected cells indicated that it was retained in the ER, with additional accumulation in the perinuclear globular structure (compare Fig. 3E and D). These results indicate that TuMV infection not only has important consequences for the morphology of the ER and Golgi apparatus but also has an impact on the secretory pathway by blocking protein secretion at the ER-Golgi interface.

The globular structure is not an isolated subcellular compartment. TuMV peripheral vesicles travel along microfilaments (15), ER transvacuolar strands, and tubules (see Movie S1 in the supplemental material), but the perinuclear globular structure is generally a static entity. However, the ER and Golgi apparatus are highly dynamic organelles, constantly undergoing remodeling (9, 39). Since the perinuclear globular structure observed in infected cells contains an amalgam of condensed ER and Golgi membranes, we wanted to investigate whether this compartment is nevertheless functionally linked to the bulk of nonmodified endomembranes. We consequently performed a fluorescence recovery after photobleaching (FRAP) experiment on TuMV-infected cells expressing ST-GFP. In one experiment, we selected a cell harboring two distinct globular structures around the nucleus and we used a 488-nm laser at high intensity to bleach the ST-GFP and $6K_2$-mCherry fluorophores in one of the two globular structures. We then monitored fluorescence recovery and redistribution every 10 s for 5 min. As shown in Fig. 4 and Movie S2 in the supplemental material, the recovery of $6K_2$-mCherry fluorescence did not occur over the 5-min time period, but ST-GFP fluorescence returned to near prebleach level within less than 2 min. In another experiment, we bleached half of the globular structure and observed the same results (data not shown).

Photoactivable GFP (PAGFP) is used for fluorescent pulse-labeling of fusion proteins at a specific position within a cell, which allows their subsequent cellular redistribution to be monitored. PAGFP fused to the *A. thaliana* ER-resident protein calnexin (CX-PAGFP) (46) was used to monitor the dynamics of the ER membrane with reference to the globular structure in TuMV-infected cells. Expression of CX-PAGFP in TuMV-infected cells that produced $6K_2$-mCherry was observed by confocal microscopy 4 days after agroinfiltration of *N. benthamiana* plants. Photoactivation was performed in an area close to or within the globular structure in a 10- to 20-s pulse, and activated CX-PAGFP distribution was followed by time-lapse photography. The localized background level of green fluorescence observed prior to activation is attributed to the high concentration of CX-PAGFP in the globular structure. Following activation in an area next to the globular structure (Fig. 5A), CX-PAGFP fluorescence drastically increased and was found to move rapidly away from the site of activation toward the cortical ER and also into the globular struc-

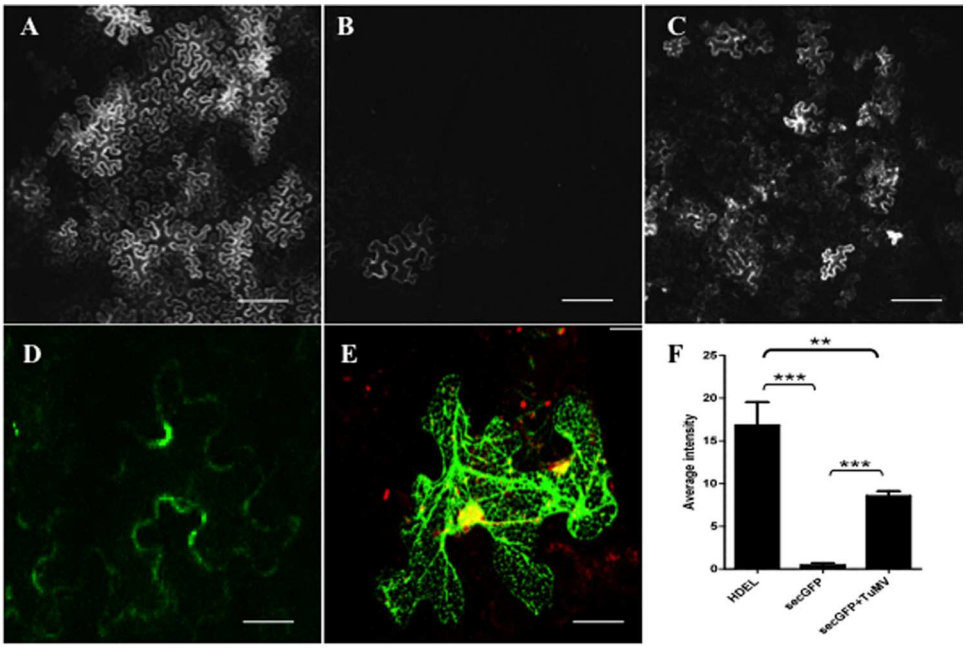

FIG 3 TuMV infection inhibits the secretion of secGFP. (A to C) Single-slice confocal microscopy images at a low magnification of leaf epidermal cells of *N. benthamiana* expressing GFP-HDEL (A), secGFP (B), and secGFP and TuMV (C). Bars = 200 μm. (D and E) Confocal microscopy images at a high magnification showing the distribution of secGFP expressed in healthy cells (D) or in infected cells producing $6K_2$-mCherry (E). Panels D and E are three-dimensional renderings of 40 1-μm-thick slices that overlap by 0.5 μm. Bars = 20 μm. (F) Average GFP fluorescence intensity of *N. benthamiana* epidermal cells expressing the indicated proteins. Statistical differences are indicated by brackets and asterisks as follows: **, $0.001 < P$ value < 0.01 (very significant); ***, P value < 0.001 (extremely significant).

ture. After less than 1 min, the fluorescence from CX-PAGFP became weak at the site of activation and in the globular structure, suggesting rapid depletion of the pulsed activated protein. When activation was performed within the globular structure (Fig. 5B), activated CX-PAGFP fluorescence was seen to rapidly fill up and then to exit the globular structure toward the cortical ER. Throughout a 15-min observation period, the fluorescence due to CX-PAGFP remained high in the globular structure, indicating that this compartment is a reservoir that can hold a large quantity of ER membranes.

These data indicate that the perinuclear globular structure was not restocked in viral components, with no input of viral proteins from nearby perinuclear structures following photobleaching. On the other hand, the TuMV-induced globular structures were dynamically connected to the bulk of the ER and Golgi apparatus. The ER, although amalgamated with Golgi bodies and compacted in the globular structure, still retained its dynamic membrane properties and moved in and out of the virus-induced compartment.

The globular structure is functionally linked to motile peripheral $6K_2$ vesicles. $6K_2$ was also fused to PAGFP ($6K_2$-PAGFP) and expressed in TuMV-infected *N. benthamiana* cells that produced $6K_2$-mCherry. Weak localized background of green fluorescence was observed in the globular structure prior to activation, probably due to the high concentration of $6K_2$-PAGFP in the structure (Fig. 6A). Photoactivation was performed for 10 to 20 s within the globular structure, and the dynamics of activated $6K_2$-PAGFP was then monitored by time-lapse photography (Fig. 6A). Following activation, $6K_2$-PAGFP fluorescence was found to rapidly fill up the globular structure, and after a delay of 25 s, a green fluorescing motile $6K_2$ vesicle was seen to originate and to move away from the structure. This experiment was repeated several times, and although few in numbers, vesicles exiting from the globular structure were consistently observed. When activation was performed next to the globular structure (Fig. 6B), motile vesicles were seen trafficking away or toward the globular structure. In the example provided in Fig. 6B, one vesicle was seen to move toward and subsequently exit from the globular structure. These experiments then provide evidence for a functional link between the perinuclear globular structure and peripheral $6K_2$ vesicles. Not only do the vesicles have their origin in the globular structure, but they can also be recycled back to it.

Brefeldin A does not abrogate the formation of the perinuclear globular structure. We next investigated the importance of ER-to-Golgi transport on the biogenesis of the globular structure. For this purpose, we treated cells with brefeldin A (BFA), a lactone antibiotic that primarily inhibits transport of proteins from the Golgi apparatus back to the ER (40). *N. benthamiana* leaves were agroinfected with TuMV expressing $6K_2$-GFP and were treated 66 h postinfection with DMSO or BFA at a concentration of 10 μg/ml before the globular structure could be observed. The cells were examined 24 h later by confocal microscopy. Treatment with BFA did not affect the formation of the perinuclear globular structure (Fig. 7C) and the production of peripheral vesicles, whose morphology was similar to that observed in untreated cells (compare the middle panels of Fig. 7A and B). However, when YFP-Sec24 was expressed in infected cells, the COPII marker punctate structures were larger and were found to be more frequently clustered with the peripheral vesicles (Fig. 7B) than in the absence of the drug (Fig. 7A). Using the JACoP plugin in ImageJ (10), the Pear-

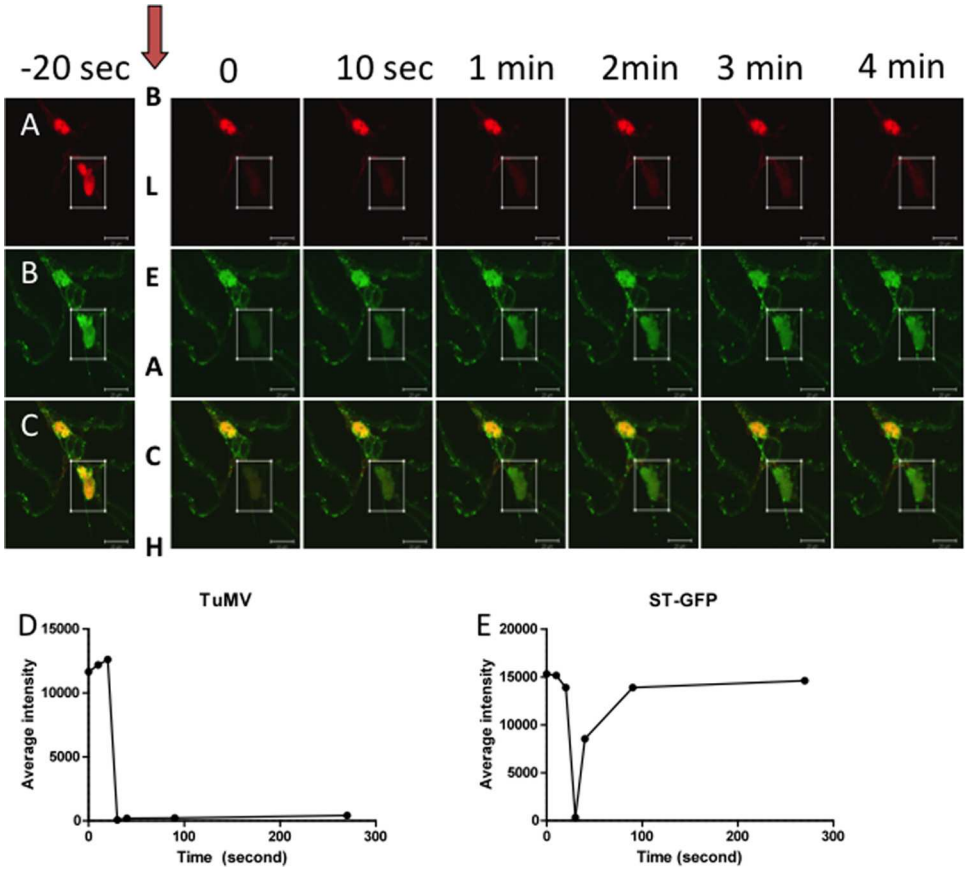

FIG 4 FRAP experiments on perinuclear globular structure. (A and B) Confocal microscopy images of leaf epidermal cells of *N. benthamiana* infected by TuMV producing $6K_2$-tagged vesicles (A) and ST-GFP (B). T (C) Merged images from panels A and B. A cell harboring two different globular structures was chosen, and at time point $T-10$ s, a rectangular region corresponding to a globular structure was bleached by a 488-nm laser for 10 s. Images were collected every 10 s. The numbers at the top of the figure show the time when fluorescence was recorded. Bars = 20 μm. (D and E) Average intensity of fluorescence emitted by $6K_2$-mCherry (D) and ST-GFP (E) before bleaching or during the recovery period.

son's correlation coefficient Rr values were 0.38 ± 0.02 and 0.14 ± 0.02 in the presence or absence of BFA, respectively (Fig. 7D), which confirms increased clustering of $6K_2$ vesicles with the COPII marker after BFA treatment.

BFA was shown to decrease the yield of TuMV particles produced during infection (56), but the assays used could not differentiate between inhibition of viral RNA replication/synthesis or inhibition of virus cell-to-cell movement. In order to discriminate between agroinfiltrated primary infected cells from secondary infected cells and thus assaying for viral intercellular movement, we introduced a gene cassette encoding GFP-HDEL under the control of the cauliflower mosaic virus (CaMV) 35S promoter next to the TuMV cassette expressing $6K_2$-mCherry, both of which are flanked by the left and right borders of the T-DNA in pCambia (Fig. 7E). Since both gene cassettes are delivered in the same cells and GFP-HDEL does not move between cells (4), primary infection foci were characterized by concomitant green and red fluorescence, while secondary infection foci exhibited red fluorescence only (Fig. 7F). No delay in virus infection and virus production was observed with this additional gene cassette, and cell-to-cell movement was observed 4 days after agroinfiltration (M. Agbeci et al., unpublished data manuscript in preparation). *N. benthamiana* leaves were agroinfiltrated with the TuMV-$6K_2$mCherry/GFP-HDEL dual-cassette construct and were treated with DMSO or BFA at a concentration of 10 μg/ml 66 h postinfiltration. The treated leaf cells were examined 24 h later by confocal microscopy with a 10× objective. Virus cell-to-cell movement was readily observed in leaves treated with DMSO but was inhibited in BFA-treated leaf samples (compare Fig. 7F and G). The surface area for foci expressing mCherry only ($n = 20$) was quantified, and the data indicated higher average intensity fluorescence for leaves treated with DMSO than for leaves treated with BFA (Fig. 7H). In the case of primary infection foci, no difference in mCherry fluorescence intensity was detected between the two treatments (data not shown), suggesting that viral replication was unaffected by the drug. Since BFA may have unexpected effects on other cellular transport pathways, we repeated the experiment by expressing along with TuMV the dominant-negative Arf1 mutant (43), which primarily inhibits Golgi recycling back to the ER. Expression of this mutant had the same inhibitory effect on TuMV cell-to-cell movement as BFA did (Fig. 7I to K). Since the dominant Arf1 had the same effect as BFA, the globular structure was still observed. The above data suggest that the secretory pathway is not required for the formation of the TuMV-induced perinuclear structure and viral protein production. On the other hand, disruption of ER-to-Golgi transport caused the retention of $6K_2$ vesicles with COPII coatamers and blocked virus cell-to-cell movement.

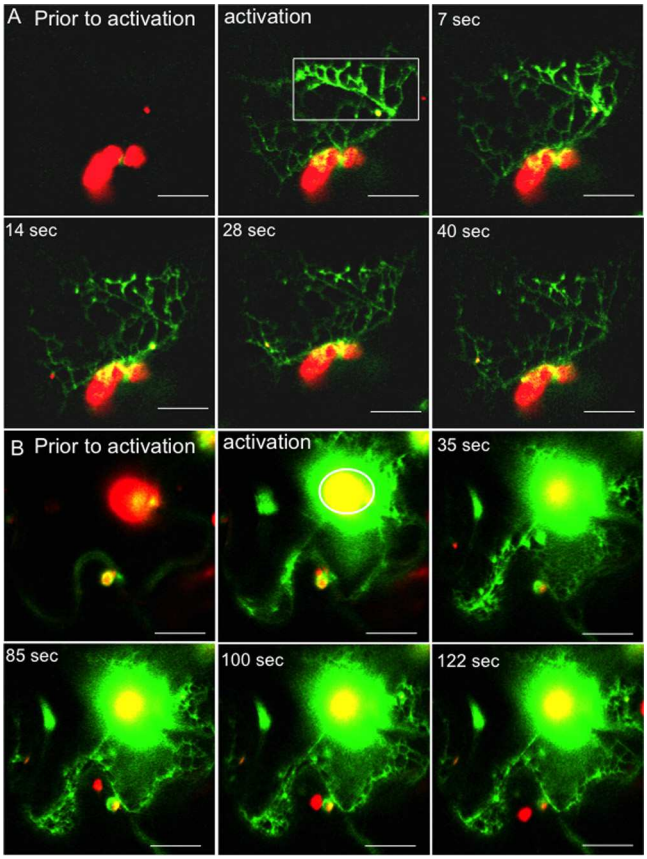

FIG 5 Photoactivation of CX-PAGFP shows connection between the globular structure induced by TuMV and the ER. Time series images of cells infected with TuMV expressing $6K_2$-mCherry showing dispersal of calnexin fused to photoactivatable GFP (CX-PAGFP) after activation with a 405-nm laser by 10 to 15 iterations using the bleach mode of the LSM 510 Meta confocal microscope (Zeiss). Activation was performed in an area next to the globular structure (A) or within the globular structure (B). The white rectangle in panel A and the white circle in panel B outline the activation area. Bars = 10 μm.

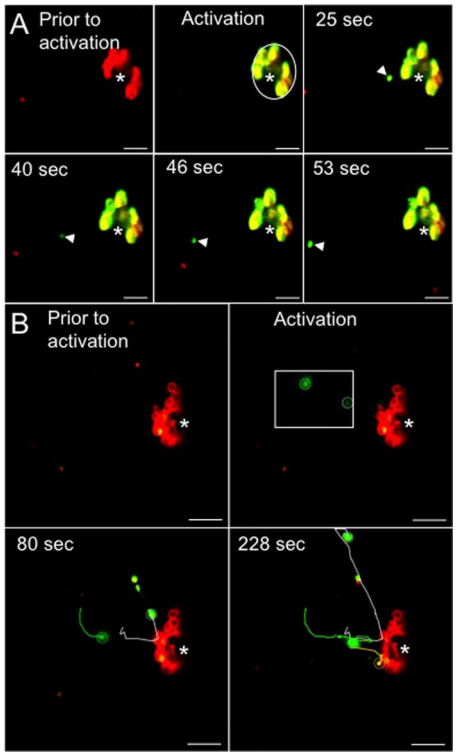

FIG 6 The globular structure is functionally linked to motile $6K_2$ vesicles. Time series images of $6K_2$-PAGFP expressed in TuMV-infected *N. benthamiana* cells that produced $6K_2$-mCherry. (A) Activation of $6K_2$-PAGFP occurred within the globular structure, and time lapse images were taken. The white arrowhead shows the movement of one vesicle originating from the globular structure. (B) Activation was performed next to the globular structure in the cytoplasm, and the movement of activated $6K_2$-PAGFP vesicles is shown using the plugin MTrackJ of ImageJ. The white circle in the Activation panel in panel A and the white rectangle in the Activation panel in panel B represent the activation spot. The circle around the vesicle shows the position at the indicated time. Bars = 10 μm.

DISCUSSION

It was previously shown that the $6K_2$ protein of TuMV induced the production of membrane-associated vesicular structures (5, 15, 17, 25, 53, 56). In the present investigation, we have investigated the impact of this production on the endomembranes of the early secretory pathway. The formation of a virus-induced perinuclear globular structure was characterized by the amalgamation of ER, Golgi, and COPII markers as well as chloroplasts within this structure, which also contained $6K_2$ and hence replication complex components. However, the cortical ER and the bulk of Golgi bodies were apparently not affected. Even though the ER and Golgi apparatus had lost their characteristic organization in this globular structure, they remained connected to the host secretory pathway. This connection is likely important for the generation of peripheral $6K_2$ vesicles, which have been shown to exit from the globular structure and possibly are recycled back. A similar functional link between peripheral bodies and their origin from the perinuclear ER has been noted in the case of Bamboo mosaic virus (31) and Potato mop-top virus (22), and in the latter case, recycling through the endocytic pathway has been suggested.

TuMV $6K_2$-induced structures are associated with viral RNA and contain viral replication and host proteins known to be required for virus production (5, 15, 17, 25, 53, 56). The production of endomembrane aggregates in the perinuclear region has been reported for a few plant viruses (2, 11, 35, 45, 54). For instance, Potato virus X (PVX) infection induced the formation of a single large inclusion body known as "X-body" localized next to the nucleus that contained ribosomes, virions, and the viral RNA-dependent RNA polymerase (2). Recently, Tilsner et al. (54) have shown that X-body biogenesis resulted in the reorganization and accumulation of host actin, ER, and Golgi apparatus into that structure for the compartmentalization of viral gene products needed for virus replication. Similarly, Grapevine fanleaf virus (GFLV) (45) and Cowpea mosaic virus (CPMV) (11) infection led to the redistribution of the ER to generate a perinuclear viral compartment where replication took place. It is then likely that the perinuclear structure is a major site for viral RNA replication. Curiously, Golgi bodies were not found in the perinuclear compartments for GFLV and CPMV, which is different from what is observed for TuMV and PVX. This noticeable discrepancy suggests the existence of different mechanisms for host endomembrane recruitment during infection.

One question is whether formation of the perinuclear structure is a result of redistribution of existing ER and Golgi membranes or

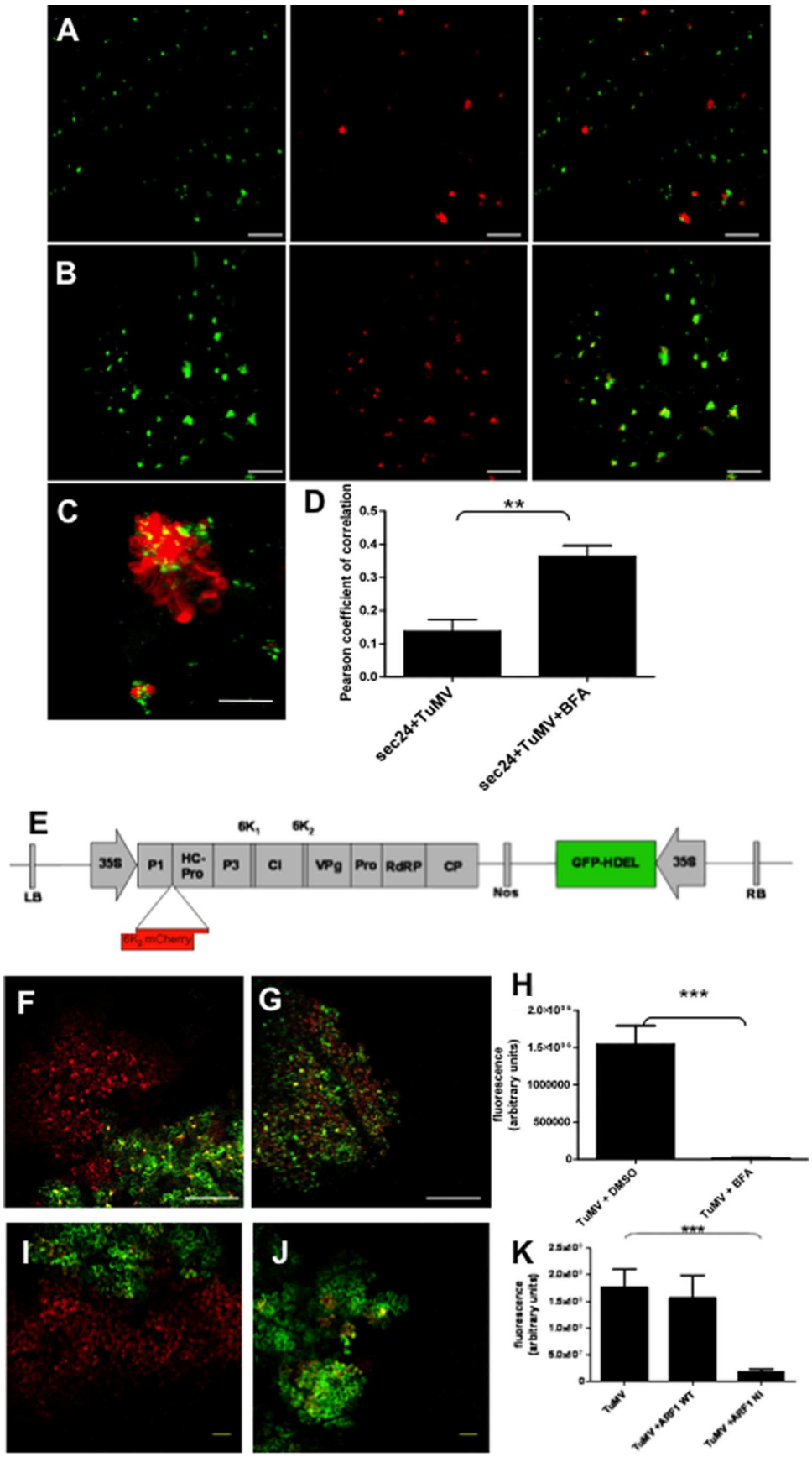
A
B
C
D
Pearson coefficient of correlation
0.5
0.4
0.3
0.2
0.1
0.0
**
sec24+TuMV
sec24+TuMV+BFA
E
6K1
6K2
35S
P1
HC-Pro
P3
CI
VPg
Pro
RdRP
CP
Nos
GFP-HDEL
35S
LB
RB
6K2 mCherry
F
G
H
***
fluorescence (arbitrary units)
2.0×10^10
1.5×10^10
1000000
500000
0
TuMV + DMSO
TuMV + BFA
I
J
K
***
fluorescence (arbitrary units)
2.5e07
2.0e07
1.5e07
1.0e07
5.0e06
0
TuMV
TuMV +ARF1 WT
TuMV +ARF1 NI

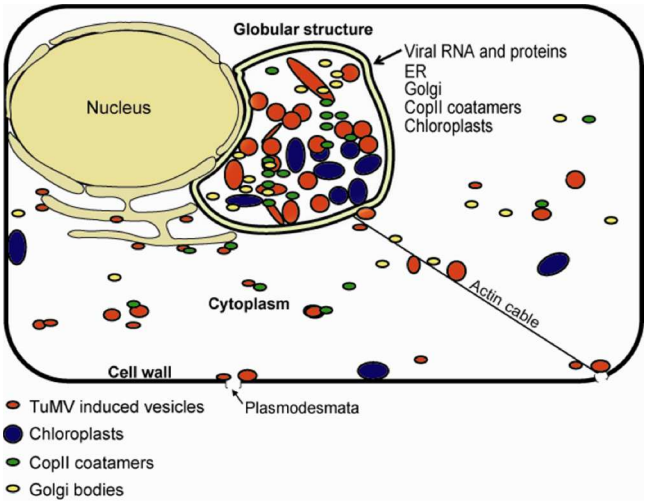

FIG 8 Model to describe the formation of the perinuclear globular structure. Early in the infection process, the incoming viral RNA is translated, and the viral gene products contribute to the formation of the perinuclear globular structure. Replication events (i.e., negative- and positive-sense RNA transcription) take place within this globular structure. After this step, viral egress is initiated by the budding of $6K_2$ vesicles at ERES in the globular structure, which then traffic along the ER/microfilaments toward the plasma membrane and plasmodesmata for ultimate delivery of the virus into neighboring cells. At that point, some peripheral vesicles may be recycled back to the globular structure.

of *de novo* synthesis. First, we did not notice any changes in the morphology of the cortical ER, and the number of Golgi bodies outside the globular structure appeared to be of the same order, whether the cell was infected or not. Additionally, the lack of depletion of CX-GFP fluorescence over an extended period (at least 15 min) when activation was done within the structure suggests that the globular structure is a large reservoir of ER membranes. Finally, it has been reported that plant viral infections stimulate *de novo* membrane synthesis (2, 11, 32, 45). These observations would suggest that the recruitment of organelles into the TuMV globular structure results from an increase in ER and Golgi synthesis, which would reflect a need for s the sustained high synthetic activity that is required for virus production.

Interestingly, aberrant perinuclear globular structures entwined by actin cables and composed of ER, Golgi apparatus, and soluble secreted markers were also observed in mutant *A. thaliana* lines (18, 38). These lines have a defect in one of the Sec24 isomers that causes a partial loss of function for the binding of cargo protein destined for secretion. The mutation led to impaired traffic of proteins at the ER-Golgi interface, accompanied with the formation of aberrant endomembrane clusters near the nucleus. These clusters are morphologically and dynamically very similar to those observed in TuMV-infected cells. Inhibition of protein transport at the ER and Golgi interface has been noted during vertebrate RNA virus infections (13, 14, 37, 50). The Norwalk virus nonstructural p22 and the picornaviral 3A and/or 2BC proteins are responsible for this phenomenon. In the case of p22, a YXΦESDG motif that mimics a diacidic ER export signal plays a critical role as an ER/Golgi trafficking antagonist (50). Alternatively, the 3A protein inhibits GBF1, a guanine nucleotide exchange factor that activates small Arf1 GTPase involved in COPI vesicle formation (59). In the case of TuMV, we also think that the inhibition of protein secretion is a consequence of viral modification of the ER-Golgi interface. The TuMV $6K_2$ protein shares some characteristics with these viral proteins (e.g., presence of a transmembrane domain responsible for vesicle formation) and may have an ER export signal (33). It will be interesting to investigate whether $6K_2$ targets a component of the early secretory pathway at the ER-Golgi interface that leads to inhibition of protein secretion and formation of the perinuclear globular structure.

BFA treatment or the coexpression of a dominant-negative mutant of Arf1 did not affect the formation of the globular structure or the production of viral proteins in primary infected cells, suggesting that viral replication proceeded normally. It thus appears that the ER-Golgi interface does not play a direct role in the globular structure morphogenesis or functionality. This situation is analogous to what has been observed during coronavirus infection where virus-induced remodeling of endoplasmic reticulum membranes and viral replication, albeit reduced, still took place in the presence of BFA (28). Additionally, production of peripheral $6K_2$ vesicles was not affected, although they showed increased overlap with the COPII marker Sec24. The importance of the secretory pathway for viral movement protein-induced vesicle trafficking and for intercellular virus movement has been demonstrated for many plant viruses (1, 20, 21, 35). In the case of Poa semilatent virus, trafficking may involve an unconventional mechanism, since treatment with secretory pathway inhibitors had no detectable effect on peripheral body formation (49). This is analogous to what we observed in the case of TuMV, but the increased clustering of Sec24 with the peripheral vesicles indicates that the latter may have become dysfunctional. This suggests that disruption of the early secretory pathway slows down the budding of $6K_2$ vesicles at ERES, which is then reflected in the inhibition of virus intercellular movement.

On the basis of the data generated in the present investigation,

FIG 7 Effect of BFA treatment on the formation of $6K_2$-tagged vesicles and on virus cell-to-cell movement. (A and B) *N. benthamiana* leaves were infiltrated with *A. tumefaciens* containing plasmids with genes encoding TuMV producing $6K_2$-mCherry-tagged vesicles and YFP-Sec24. The leaves were infiltrated with DMSO (A) or 10 μg/ml BFA (B) 66 h after agroinfiltration. The cells were analyzed 24 h later with a LSM 510 Meta confocal microscope (Zeiss). The left panels show the green fluorescence channel for YFP-Sec24, the middle panels show the red fluorescence channel for TuMV producing $6K_2$-mCherry-tagged vesicles, and the right panels show the merged images. The images are three-dimensional (3D) renderings of 15 1-μm-thick slices that overlap by 0.5 μm. (C) Image showing that the globular structure is produced in the presence of BFA. (D) Quantification of clustering between YFP-Sec24 COPII marker and the $6K_2$-mCherry-tagged vesicles by calculation of the Pearson's correlation coefficient Rr values. (E) Schematic representation of the plasmid used to discriminate primary agroinfiltrated infected cells from secondary infected cells. Primary infection foci are characterized by concomitant green and red fluorescence, while secondary infection foci show red fluorescence only. (F and G) Viral movement was assayed in the absence (F) or presence (G) of BFA. (H) The surface area of only the foci with red fluorescence was calculated and expressed in arbitrary fluorescence units. (I and J) The effect of Arf1 expression on virus cell-to-cell movement was assayed in the presence of wild-type Arf1 (I) or in the presence of the dominant-negative mutant NI of Arf1 (J). (K) The surface area of only the foci with red fluorescence was calculated and expressed in arbitrary fluorescence units. Statistical differences are indicated by brackets and asterisks as follows: **, $0.001 < P$ value < 0.01 (very significant); ***, P value < 0.001 (extremely significant).

we suggest the following model to describe cellular remodeling during TuMV infection (Fig. 8). Early in the infection process, the incoming viral RNA is translated and the viral gene products contribute to the formation of the perinuclear globular structure. Replication events (i.e., negative- and positive-sense RNA transcription) take place within this globular structure, and these events would still happen even if the ER-Golgi interface is disrupted during viral infection. After this step, viral egress is initiated by the budding of $6K_2$ vesicles at ERES in the globular structure, which then traffic along the ER/microfilaments toward the plasma membrane and plasmodesmata for ultimate delivery of the virus into neighboring cells. At that point, some peripheral vesicles may be recycled back to the globular structure. Future investigations will aim at identifying host proteins that are involved in the formation of the perinuclear structure and why in the absence of MTOC, such a large viral structure can be formed near the nucleus.

ACKNOWLEDGMENTS

We thank M. Desrosiers and J. Lacoste for helping with confocal microscopy, C. Hawes for ERD2-GFP, and J. Runions for CX-PAGFP. We thank H. Sanfaçon for critically reading the manuscript.

This study was supported by the Natural Sciences and Engineering Research Council of Canada and from Le Fonds de recherche du Québec – Nature et technologies to H.Z. and J.-F.L.

REFERENCES

1. **Amari K, Lerich A, Schmitt-Keichinger C, Dolja VV, Ritzenthaler C.** 2011. Tubule-guided cell-to-cell movement of a plant virus requires class XI myosin motors. PLoS Pathog. **7**:e1002327. doi:10.1371/journal.ppat.1002327.
2. **Bamunusinghe D, et al.** 2009. Analysis of potato virus X replicase and TGBp3 subcellular locations. Virology **393**:272–285.
3. **Bamunusinghe D, Seo J-K, Rao ALN.** 2011. Subcellular localization and rearrangement of endoplasmic reticulum by brome mosaic virus capsid protein. J. Virol. **85**:2953–2963.
4. **Batoko H, Zheng HQ, Hawes C, Moore I.** 2000. A rab1 GTPase is required for transport between the endoplasmic reticulum and Golgi apparatus and for normal Golgi movement in plants. Plant Cell **12**:2201–2218.
5. **Beauchemin C, Boutet N, Laliberté J-F.** 2007. Visualization of the interaction between the precursors of VPg, the viral protein linked to the genome of Turnip mosaic virus, and the translation eukaryotic initiation factor iso 4E in planta. J. Virol. **81**:775–782.
6. **Belov GA, et al.** 2007. Hijacking components of the cellular secretory pathway for replication of poliovirus RNA. J. Virol. **81**:558–567.
7. **Belov GA, Feng Q, Nikovics K, Jackson CL, Ehrenfeld E.** 2008. A critical role of a cellular membrane traffic protein in poliovirus RNA replication. PLoS Pathog. **4**:e1000216. doi:10.1371/journal.ppat.1000216.
8. **Belov GA, et al.** 2012. Complex dynamic development of poliovirus membranous replication complexes. J. Virol. **86**:302–312.
9. **Boevink P, et al.** 1998. Stacks on tracks: the plant Golgi apparatus traffics on an actin/ER network. Plant J. **15**:441–447.
10. **Bolte S, Cordelieres FP.** 2006. A guided tour into subcellular colocalization analysis in light microscopy. J. Microsc. (Oxford) **224**:213–232.
11. **Carette JE, Stuiver M, Van Lent J, Wellink J, Van Kammen AB.** 2000. Cowpea mosaic virus infection induces a massive proliferation of endoplasmic reticulum but not Golgi membranes and is dependent on de novo membrane synthesis. J. Virol. **74**:6556–6563.
12. **Chen J, Stefano G, Brandizzi F, Zheng H.** 2011. Arabidopsis RHD3 mediates the generation of the tubular ER network and is required for Golgi distribution and motility in plant cells. J. Cell Sci. **124**:2241–2252.
13. **Choe SS, Dodd DA, Kirkegaard K.** 2005. Inhibition of cellular protein secretion by picornaviral 3A proteins. Virology **337**:18–29.
14. **Cornell CT, Kiosses WB, Harkins S, Whitton JL.** 2006. Inhibition of protein trafficking by coxsackievirus b3: multiple viral proteins target a single organelle. J. Virol. **80**:6637–6647.
15. **Cotton S, et al.** 2009. Turnip mosaic virus RNA replication complex vesicles are mobile, align with microfilaments, and are each derived from a single viral genome. J. Virol. **83**:10460–10471.
16. **den Boon JA, Ahlquist P.** 2010. Organelle-like membrane compartmentalization of positive-strand RNA virus replication factories. Annu. Rev. Microbiol. **64**:241–256.
17. **Dufresne PJ, et al.** 2008. Heat shock 70 protein interaction with Turnip mosaic virus RNA-dependent RNA polymerase within virus-induced membrane vesicles. Virology **374**:217–227.
18. **Faso C, et al.** 2009. A missense mutation in the Arabidopsis COPII coat protein Sec24A induces the formation of clusters of the endoplasmic reticulum and Golgi apparatus. Plant Cell **21**:3655–3671.
19. **Fu CY, Johnson JE.** 2011. Viral life cycles captured in three-dimensions with electron microscopy tomography. Curr. Opin. Virol. **1**:125–133.
20. **Harries PA, et al.** 2009. Differing requirements for actin and myosin by plant viruses for sustained intercellular movement. Proc. Natl. Acad. Sci. U. S. A. **106**:17594–17599.
21. **Harries PA, Schoelz JE, Nelson RS.** 2010. Intracellular transport of viruses and their components: utilizing the cytoskeleton and membrane highways. Mol. Plant Microbe Interact. **23**:1381–1393.
22. **Haupt S, et al.** 2005. Two plant-viral movement proteins traffic in the endocytic recycling pathway. Plant Cell **17**:164–181.
23. **Hayat MA.** 1981. Fixation for electron microscopy. Academic Press, New York, NY.
24. **Hsu N-Y, et al.** 2010. Viral reorganization of the secretory pathway generates distinct organelles for RNA replication. Cell **141**:799–811.
25. **Huang TS, Wei T, Laliberté J-F, Wang A.** 2010. A host RNA helicase-like protein, AtRH8, interacts with the potyviral genome-linked protein, VPg, associates with the virus accumulation complex, and is essential for infection. Plant Physiol. **152**:255–266.
26. **Kawakami S, Watanabe Y, Beachy RN.** 2004. Tobacco mosaic virus infection spreads cell to cell as intact replication complexes. Proc. Natl. Acad. Sci. U. S. A. **101**:6291–6296.
27. **Knoops K, et al.** 2008. SARS-coronavirus replication is supported by a reticulovesicular network of modified endoplasmic reticulum. PLoS Biol. **6**:e226. doi:10.1371/journal.pbio.0060226.
28. **Knoops K, et al.** 2010. Integrity of the early secretory pathway promotes, but is not required for, severe acute respiratory syndrome coronavirus RNA synthesis and virus-induced remodeling of endoplasmic reticulum membranes. J. Virol. **84**:833–846.
29. **Laliberté J-F, Sanfaçon H.** 2010. Cellular remodeling during plant virus infection. Annu. Rev. Phytopathol. **48**:69–91.
30. **Langenberg WG.** 1991. Cylindrical inclusion bodies of wheat streak mosaic virus and three other potyviruses only self-assemble in mixed infections. J. Gen. Virol. **72**:493–497.
31. **Lee SC, Wu CH, Wang CW.** 2010. Traffic of a viral movement protein complex to the highly curved tubules of the cortical endoplasmic reticulum. Traffic **11**:912–930.
32. **Lee WM, Ahlquist P.** 2003. Membrane synthesis, specific lipid requirements, and localized lipid composition changes associated with a positive-strand RNA virus RNA replication protein. J. Virol. **77**:12819–12828.
33. **Lerich A, Langhans M, Sturm S, Robinson DG.** 2011. Is the 6 kDa tobacco etch viral protein a bona fide ERES marker? J. Exp. Bot. **62**:5013–5023.
34. **Limpens RW, et al.** 2011. The transformation of enterovirus replication structures: a three-dimensional study of single- and double-membrane compartments. mBio **2**(5):e00166–11. doi:10.1128/mBio.00166-11.
35. **Liu JZ, Blancaflor EB, Nelson RS.** 2005. The tobacco mosaic virus 126-kilodalton protein, a constituent of the virus replication complex, alone or within the complex aligns with and traffics along microfilaments. Plant Physiol. **138**:1853–1865.
36. **Marti L, Fornaciari S, Renna L, Stefano G, Brandizzi F.** 2010. COPII-mediated traffic in plants. Trends Plant Sci. **15**:522–528.
37. **Moffat K, et al.** 2007. Inhibition of the secretory pathway by foot-and-mouth disease virus 2BC protein is reproduced by coexpression of 2B with 2C, and the site of inhibition is determined by the subcellular location of 2C. J. Virol. **81**:1129–1139.
38. **Nakano RT, et al.** 2009. GNOM-LIKE1/ERMO1 and SEC24a/ERMO2 are required for maintenance of endoplasmic reticulum morphology in Arabidopsis thaliana. Plant Cell **21**:3672–3685.
39. **Nebenfuhr A, et al.** 1999. Stop-and-go movements of plant Golgi stacks are mediated by the acto-myosin system. Plant Physiol. **121**:1127–1142.
40. **Nebenfuhr A, Ritzenthaler C, Robinson DG.** 2002. Brefeldin A: deciphering an enigmatic inhibitor of secretion. Plant Physiol. **130**:1102–1108.

41. **Nelson BK, Cai X, Nebenfuhr A.** 2007. A multicolored set of in vivo organelle markers for co-localization studies in Arabidopsis and other plants. Plant J. **51**:1126–1136.
42. **Netherton CL, Wileman T.** 2011. Virus factories, double membrane vesicles and viroplasm generated in animal cells. Curr. Opin. Virol. **1**:381–387.
43. **Phillipson BA, et al.** 2001. Secretory bulk flow of soluble proteins is efficient and COPII dependent. Plant Cell **13**:2005–2020.
44. **Ritzenthaler C.** 2011. Parallels and distinctions in the direct cell-to-cell spread of the plant and animal viruses. Curr. Opin. Virol. **1**:403–409.
45. **Ritzenthaler C, et al.** 2002. Grapevine fanleaf virus replication occurs on endoplasmic reticulum-derived membranes. J. Virol. **76**:8808–8819.
46. **Runions J, Brach T, Kuhner S, Hawes C.** 2006. Photoactivation of GFP reveals protein dynamics within the endoplasmic reticulum membrane. J. Exp. Bot. **57**:43–50.
47. **Saint-Jore CM, et al.** 2002. Redistribution of membrane proteins between the Golgi apparatus and endoplasmic reticulum in plants is reversible and not dependent on cytoskeletal networks. Plant J. **29**:661–678.
48. **Schaad MC, Jensen PE, Carrington JC.** 1997. Formation of plant RNA virus replication complexes on membranes: role of an endoplasmic reticulum-targeted viral protein. EMBO J. **16**:4049–4059.
49. **Schepetilnikov MV, et al.** 2008. Intracellular targeting of a hordeiviral membrane-spanning movement protein: sequence requirements and involvement of an unconventional mechanism. J. Virol. **82**:1284–1293.
50. **Sharp TM, Guix S, Katayama K, Crawford SE, Estes MK.** 2010. Inhibition of cellular protein secretion by Norwalk virus nonstructural protein p22 requires a mimic of an endoplasmic reticulum export signal. PLoS One **5**:e13130. doi:10.1371/journal.pone.0013130.
51. **Sparkes IA, Ketelaar T, De Ruijter NCA, Hawes C.** 2009. Grab a Golgi: laser trapping of Golgi bodies reveals in vivo interactions with the endoplasmic reticulum. Traffic **10**:567–571.
52. **Suhy DA, Giddings TH, Jr, Kirkegaard K.** 2000. Remodeling the endoplasmic reticulum by poliovirus infection and by individual viral proteins: an autophagy-like origin for virus-induced vesicles. J. Virol. **74**:8953–8965.
53. **Thivierge K, et al.** 2008. Eukaryotic elongation factor 1A interacts with Turnip mosaic virus RNA-dependent RNA polymerase and VPg-Pro in virus-induced vesicles. Virology **377**:216–225.
54. **Tilsner J, et al.** 2012. The TGB1 movement protein of potato virus X reorganizes actin and endomembranes into the X-Body, a viral replication factory. Plant Physiol. **158**:1359–1370.
55. **Verchot J.** 2011. Wrapping membranes around plant virus infection. Curr. Opin. Virol. **1**:388–395.
56. **Wei T, et al.** 2010. Sequential recruitment of the endoplasmic reticulum and chloroplasts for plant potyvirus replication. J. Virol. **84**:799–809.
57. **Wei T, Wang A.** 2008. Biogenesis of cytoplasmic membranous vesicles for plant potyvirus replication occurs at endoplasmic reticulum exit sites in a COPI- and COPII-dependent manner. J. Virol. **82**:12252–12264.
58. **Welsch S, et al.** 2009. Composition and three-dimensional architecture of the Dengue virus replication and assembly sites. Cell Host Microbe **5**:365–375.
59. **Wessels E, et al.** 2006. A viral protein that blocks Arf1-mediated COP-I assembly by inhibiting the guanine nucleotide exchange factor GBF1. Dev. Cell **11**:191–201.
60. **Wolk B, Buchele B, Moradpour D, Rice CM.** 2008. A dynamic view of hepatitis C virus replication complexes. J. Virol. **82**:10519–10531.
61. **Zheng H, et al.** 2005. A Rab-E GTPase mutant acts downstream of the Rab-D subclass in biosynthetic membrane traffic to the plasma membrane in tobacco leaf epidermis. Plant Cell **17**:2020–2036.
62. **Zheng H, Kunst L, Hawes C, Moore I.** 2004. A GFP-based assay reveals a role for RHD3 in transport between the endoplasmic reticulum and Golgi apparatus. Plant J. **37**:398–414.